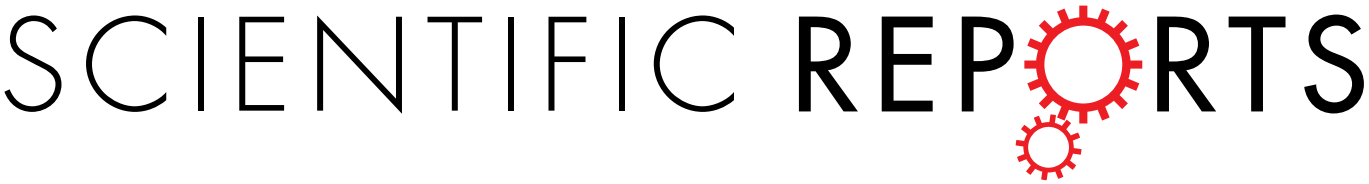

OPEN

Photonic topological phases in dispersive metamaterials

You-Zhong Yu & Ruey-Lin Chern

Received: 6 June 2018
Accepted: 15 November 2018
Published online: 14 December 2018

We analyze the photonic topological phases in dispersive metamaterials which satisfy the degenerate condition at a reference frequency. The electromagnetic duality allows for the hybrid modes to be decoupled and described by the spin-orbit Hamiltonians with pseudospin 1, which result in nonzero spin Chern numbers that characterize the topological phases. In particular, the combined Hamiltonian of the hybrid modes complies with a fermionic-like pseudo time-reversal symmetry that ensures the Kramers degeneracy, leading to the topological protection of helical edge states. The transverse spin generated by the evanescent surface waves is perpendicular to the wave vector, which exhibits the spin-momentum locking as in the surface states for three-dimensional topological insulators. The topological properties of the helical edge states are further illustrated with the robust transport of a pair of counterpropagating surface waves with opposite polarization handedness at an irregular boundary of the metamaterial.

Inspired by the discovery of topological insulators in recent years[1–7], there has been a surge of interest in the study of topological phases in photonic systems[8–23]. Topological insulators are insulating in the bulk but possess conducting states on their surfaces. The role of topology was first established in the study of phase transition in two-dimensional (2D) systems, known as the Kosterlitz-Thouless transition[24]. A well understood form of the topological phase was later represented by the quantum Hall (QH) state[25], a 2D electron gas in a static magnetic field, which belongs to a topological class that breaks the time-reversal (TR) symmetry. In this system, a single edge mode, known as the *chiral* edge state, propagates unidirectionally at the boundary, which is insensitive to disorder[26]. The topological properties of the QH states are manifest on the quantized Hall conductance characterized by the TKNN invariant or Chern number[27].

Another topological phase that preserves the TR symmetry is the quantum spin Hall (QSH) state[28–30], in which no magnetic field is required. The spin-orbit interaction allows a different topological class when the TR symmetry is unbroken. In this system, a pair of edge modes with opposite spin, known as the *helical* edge states, counterpropagate at a given edge without backscattering[31]. The topological properties of the QSH states can be characterized by the Z_2 invariant[32] or spin Chern number[33]. The theoretical concepts developed in the QSH states were soon generalized to three-dimensional (3D) topological insulators[1,2].

The photonic analogue of the QH states was identified in 2D gyroelectric or gyromagnetic photonic crystals[8–10], where the gyrotropy effect breaks the TR symmetry as a static magnetic field does in the QH system. The unidirectional edge modes, which are analogous to the chiral edge states, exist in the photonic band gap with a nonzero Chern number for all bands below the gap. More recently, the photonic QH states can also be found in the Tellegen metacrystals[34]. In another aspect, the photonic QSH states were demonstrated in 2D bianisotropic photonic crystals[15,21], where the magnetoelectric coupling emulates the effect of spin-orbit interaction. The counterpropagating edge modes, which are analogous to the helical edge states in the QSH system, exist in the frequency gap between the bulk bands with nonzero spin Chern numbers.

The helical edge states, which are doubly degenerate and TR partners of each other, form a Kramers doublet that usually exists in a TR invariant system with spin 1/2. The Kramers degeneracy, which is crucial to the emergence of helical edge states, therefore cannot readily apply to the photonic system with spin 1, unless additional symmetry has been imposed in the system. For the bianisotropic medium with the 'spin'-degenerate condition: $\varepsilon = \mu$[15,35–37], the transverse magnetic (TM) and transverse electric (TE) modes propagate with identical wave numbers. The linear combinations $E_z \pm H_z$, referred to as the *pseudospin* states, become a Kramers doublet in the photonic system[15]. The spin-degenerate condition was also used in the Tellegen medium for constructing the Kramers degeneracy, where the pseudospin states are expressed as $E_z \pm iH_z$[21]. Furthermore, the hybridization of TM and TE modes was used to create the photonic topological phases in metacrystal waveguides[17,19,38–41]. The

Institute of Applied Mechanics, National Taiwan University, Taipei, 106, Taiwan. Correspondence and requests for materials should be addressed to R.-L.C. (email: chernrl@ntu.edu.tw)

Kramers degeneracy may even exist in 2D dielectric photonic crystals[20,42,43] without the hybridization of TM and TE modes, where the pseudospin states are represented by the combination of *p* and *d* orbital-like basis functions. In photonic systems, the Kramers degeneracy is guaranteed by the *pseudo* TR symmetry[20,21], which can be constructed from the symmetry in crystal structure[20,44] or constitutive relation[21].

In the present study, we analyze the photonic topological phases in dispersive metamaterials which satisfy the degenerate condition ($\underline{\varepsilon} = -\underline{\mu}$) at a reference frequency ω_0, around which a frequency gap between the bulk modes may exist. The electromagnetic duality allows for the hybrid modes ($\mathbf{E} \pm \eta_0 \mathbf{H}$) to be decoupled at the reference frequency, which are determined by two subsystems with degenerate eigenvalues. By introducing the pseudospin states as the eigenfield basis, the hybrid modes are described by the spin-orbit Hamiltonians with pseudospin 1, which result in nonzero spin Chern numbers that characterize the topological phases. In particular, the combined Hamiltonian of the two subsystems is TR invariant under a fermionic-like pseudo TR operator T_p with $T_p^2 = -\underline{I}$, which ensures the Kramers degeneracy of the hybrid modes, leading to the topological protection of helical edge states. The Kramers doublet consists of a pseudospin state from the plus hybrid mode ($\mathbf{E} + \eta_0 \mathbf{H}$) and another state from the minus hybrid mode ($\mathbf{E} - \eta_0 \mathbf{H}$), which are TR partners and orthogonal to each other.

For illumination, the surface modes at the interface between vacuum and the metamaterial are analytically formulated based on Maxwell's boundary conditions, which are represented by a dispersion surface in the frequency gap and reduced to an ellipse or a circle at the reference frequency. The evanescent surface wave generates a *transverse spin* perpendicular to the wave vector, which exhibits the spin-moment locking as in the surface states for 3D topological insulators. The topological properties of the surface modes are further illustrated with the electromagnetic radiation excited by an appropriately phased point dipole at the interface. The surface waves with opposite polarization handedness counterpropagate toward different directions, which are able to bend around sharp corners without backscattering.

Results

Bulk modes. Consider a dispersive medium characterized by the frequency-dependent permittivity tensor $\varepsilon_0 \underline{\varepsilon}(\omega)$ and permeability tensor $\mu_0 \underline{\mu}(\omega)$. Treating the combined electric field $E = (E_x, E_y, E_z)$ and magnetic field $H = (H_x, H_y, H_z)$ as a six-component vector, Maxwell's equations for the time-harmonic fields (with the convention $e^{-i\omega t}$) are written in matrix form as

$$\begin{pmatrix} \omega\underline{\varepsilon} & c\mathbf{k} \times \underline{I} \\ c\mathbf{k} \times \underline{I} & -\omega\underline{\mu} \end{pmatrix} \begin{pmatrix} \mathbf{E} \\ \mathbf{H}' \end{pmatrix} = 0, \tag{1}$$

where $\underline{I}$ is the 3×3 identity matrix, $\mathbf{H}' = \eta_0 \mathbf{H}$, and $\eta_0 = \sqrt{\mu_0/\varepsilon_0}$. Assume that the medium is uniaxially anisotropic with the material parameters: $\underline{\varepsilon} = \mathrm{diag}(\varepsilon_t, \varepsilon_t, \varepsilon_z)$ and $\underline{\mu} = \mathrm{diag}(\mu_t, \mu_t, \mu_z)$. The existence of a nontrivial solution of $\mathbf{E}$ and $\mathbf{H}'$ requires that the determinant of the 6×6 matrix in Eq. (1) be zero, which gives the characteristic equation of the bulk modes as

$$[\varepsilon_t(k_t^2 - \varepsilon_z \mu_t k_0^2) + \varepsilon_z k_z^2]\left[\mu_t(k_t^2 - \varepsilon_t \mu_z k_0^2) + \mu_z k_z^2\right] = 0, \tag{2}$$

where $k_t^2 = k_x^2 + k_y^2$ and $k_0 = \omega/c$. The above bi-quadratic equation shows that the bulk modes consist of two parts with dual symmetry between ε_n and μ_n ($n = t, z$).

For analyzing the topological phases in the present medium, we assume that the medium satisfies the 'degenerate' condition: $\underline{\varepsilon} = -\underline{\mu}$ at a reference frequency ω_0. In the neighborhood of ω_0, ε_n and μ_n can be approximated, respectively, as $\varepsilon_n \approx \varepsilon_{n0} + \left.\frac{d\varepsilon_n}{d\omega}\right|_{\omega=\omega_0} (\omega - \omega_0) \equiv \varepsilon_{n0} + \widetilde{\varepsilon}_n \delta\omega/\omega_0$ and $\mu_n \approx \mu_{n0} + \left.\frac{d\mu_n}{d\omega}\right|_{\omega=\omega_0} (\omega - \omega_0) \equiv \mu_{n0} + \widetilde{\mu}_n \delta\omega/\omega_0$. If $\varepsilon_{t0}\varepsilon_{z0} \neq 0$ ($\mu_{t0}\mu_{z0} \neq 0$), a frequency gap between the two bulk modes exists around ω_0. The band gap size can be estimated by the solutions of ω at $k_t = k_z = 0$ [cf. Eq. (2)], between which the bulk modes do not exist. For $\varepsilon_{n0} < 0$ ($\mu_{n0} > 0$), the upper and lower band edges are approximated by $\omega/\omega_0 \approx 1 + \min(-\varepsilon_{t0}/\widetilde{\varepsilon}_t, -\varepsilon_{z0}/\widetilde{\varepsilon}_z)$ and $\omega/\omega_0 \approx 1 - \min(\mu_{t0}/\widetilde{\mu}_t, \mu_{z0}/\widetilde{\mu}_z)$, respectively. Here, $\widetilde{\varepsilon}_t$, $\widetilde{\varepsilon}_z$, $\widetilde{\mu}_t$, and $\widetilde{\mu}_z$ are assumed to be positive definite[45].

Spin-orbit Hamiltonians. The electromagnetic duality of Maxwell's equations dictates that the matrix in Eq. (1) is symmetric with the same diagonal elements when the degenerate condition is satisfied. This enables us to rewrite the wave equations for the hybrid modes, defined by $\mathbf{E} \pm \mathbf{H}'$, at the reference frequency as

$$\begin{pmatrix} \mathcal{H}_0(\mathbf{k}) & 0 \\ 0 & \mathcal{H}_0(-\mathbf{k}) \end{pmatrix} \begin{pmatrix} \mathbf{E} + \mathbf{H}' \\ \mathbf{E} - \mathbf{H}' \end{pmatrix} = 0, \tag{3}$$

where $\mathcal{H}_0(\pm\mathbf{k}) = \omega\underline{\varepsilon} \pm c\mathbf{k} \times \underline{I}$. Note that the hybrid modes are completely decoupled and determined by two subsystems (3×3 matrix) with the same eigenvalues, their matrix determinants being equal: $|\mathcal{H}_0(\mathbf{k})| = |\mathcal{H}_0(-\mathbf{k})|$. In the isotropic case, where $\varepsilon_{t0} = \varepsilon_{z0} \equiv \varepsilon$ and $\widetilde{\varepsilon}_t = \widetilde{\varepsilon}_z \equiv \widetilde{\varepsilon}$, the wave equation for the plus hybrid mode $\mathbf{F} = \mathbf{E} + \mathbf{H}'$ can be rearranged as (see Methods A)

$$\mathcal{H}_+ \psi - d\psi = \delta\omega\psi, \tag{4}$$

by introducing the *pseudospin* state $\psi = U^{-1}\widetilde{\psi}$, where $\widetilde{\psi} = \left(\frac{-F_x + iF_y}{\sqrt{2}}, F_z, \frac{F_x + iF_y}{\sqrt{2}}\right)^T$ and $U = \mathrm{diag}(\sqrt{\widetilde{\varepsilon}_z/\widetilde{\varepsilon}_t}, 1, \sqrt{\widetilde{\varepsilon}_z/\widetilde{\varepsilon}_t})$. In Eq. (4), $d = \omega_0\varepsilon/\widetilde{\varepsilon}$ and

$$\mathcal{H}_+ = \alpha \mathbf{S} \cdot \kappa, \tag{5}$$

where $\alpha = c/\tilde{\varepsilon}$, $\kappa = \kappa_x\hat{x} + \kappa_y\hat{y} + \kappa_z\hat{z} = i\mathbf{k}$, $\mathbf{S} = S_x\hat{x} + S_y\hat{y} + S_z\hat{z}$, and S_n ($n = x, y, z$) are the spin matrices for spin 1.

Note here that Eq. (4) is formulated as an eigensystem with $\delta\omega$ as the eigenvalue. The Hamiltonian $\mathcal{H}_+$ in Eq. (5) represents the spin-orbit interaction $S{\cdot}\kappa$ with pseudospin 1[45], which is mathematically equivalent to the Hamiltonian of a magnetic dipole moment in a magnetic field. The imaginary wave vector κ in $\mathcal{H}_+$ reflects the fact that the wave is evanescent in the frequency gap. For the minus hybrid mode $\mathbf{F} = \mathbf{E} - \mathbf{H}'$ in Eq. (3), it is straightforward to show that the corresponding spin-orbit Hamiltonian is given by

$$\mathcal{H}_- = -\alpha \mathbf{S} \cdot \kappa. \tag{6}$$

Note that the hybrid modes can be slightly different if the corresponding Hamiltonian is rewritten in a different format[37,46,47].

Topological invariants. The topological properties of the spin-orbit Hamiltonians $\mathcal{H}_\pm$ can be characterized by the topological invariants based on their eigenfields. For this purpose, we calculate the Berry flux over a closed surface S: $\kappa_x^2 + \kappa_y^2 + \kappa_z^2 = \varepsilon^2 k_0^2$, corresponding to the bulk mode at the reference frequency ω_0 in the imaginary wave vector space. The eigensystem for the plus hybrid mode in Eq. (5)

$$\mathcal{H}_+ \psi_\sigma = \lambda_\sigma \psi_\sigma. \tag{7}$$

is solved to give the eigenvalues λ_σ and eigenvectors ψ_σ ($\sigma = \pm 1, 0$), based on which the Chern numbers are calculated to give $C_\sigma = 2\sigma$ (see Methods B). The nonzero topological invariants C_σ ($\sigma = \pm 1$) reveal the topological nature of the pseudospin states, where σ describes the helicity (or handedness) of the states. For this subsystem, the total Chern number $C = \sum_\sigma C_\sigma$ and the spin Chern number $C_{\text{spin}} = \sum_\sigma \sigma C_\sigma$[33] are given by

$$C = 0, \;\; C_{\text{spin}} = 4, \tag{8}$$

which are consistent with the quantum spin Hall effect of light[48]. On the other hand, the eigensystem for the minus hybrid mode in Eq. (6) is given by

$$\mathcal{H}_- \psi_{-\sigma} = \lambda_\sigma \psi_{-\sigma}, \tag{9}$$

where the eigenvalues λ_σ are the same as those of $\mathcal{H}_+$. The helicity of the eigenvectors, however, has been flipped from σ to $-\sigma$. The Chern numbers are therefore change signs as $C_\sigma = -2\sigma$. For this subsystem, the total and spin Chern numbers are given by

$$C = 0, \, C_{\text{spin}} = -4. \tag{10}$$

The vanishing total Chern number C in the subsystems reflects the TR symmetry of Maxwell's equations and the absence of QH states in free photons, while the spin Chern numbers $C_{\text{spin}} = \pm 4$ indicate that there exist two pairs of QSH edge states which are doubly-degenerate with respect to the helicity σ. The existence of surface modes in Maxwell's equations, however, requires the presence of an interface (between two different media) that breaks the duality symmetry of electromagnetic fields as in an unbounded region, and therefore only one pair of edge modes survives at the interface[48]. This feature will be confirmed by the characteristic equation of surface modes at the interface between vacuum and the metamaterial.

According to Eqs (7) and (9), the eigensystem of the combined hybrid modes is written as

$$\begin{pmatrix} \mathcal{H}_+ & 0 \\ 0 & \mathcal{H}_- \end{pmatrix} \begin{pmatrix} \psi_\sigma \\ \psi_{-\sigma} \end{pmatrix} = \lambda_\sigma \begin{pmatrix} \psi_\sigma \\ \psi_{-\sigma} \end{pmatrix}, \tag{11}$$

which states that the eigenstates ψ_σ and $\psi_{-\sigma}$ of their respective subsystems are degenerate with the eigenvalue λ_σ. The combined Hamiltonian is therefore considered two copies of the spin-orbit Hamiltonian with opposite helicity. This feature will play a crucial role in constructing the Kramers degeneracy in the present problem, leading to the topological protection of helical edge states.

Pseudo time-reversal symmetry. The Hamiltonian for Maxwell's equations [cf. Eq. (1)] in a lossless medium with $\underline{\varepsilon} = \underline{\varepsilon}^*$ and $\underline{\mu} = \underline{\mu}^*$ is time-reversal (TR) invariant under T_b, that is,

$$T_b \mathcal{H}_m T_b^{-1} = \mathcal{H}_m, \;\; \mathcal{H}_m = \begin{pmatrix} \omega\underline{\varepsilon} & c\mathbf{k} \times \underline{I} \\ c\mathbf{k} \times \underline{I} & -\omega\underline{\mu} \end{pmatrix}, \tag{12}$$

where $T_b = \sigma_z K$ with $T_b^2 = \underline{I}$ is the bosonic TR operator for photons and K is the complex conjugation[18]. The Hamiltonian $\mathcal{H}_m$, however, is not TR invariant under T_f, that is, $T_f \mathcal{H}_m T_f^{-1} \neq \mathcal{H}_m$, where $T_f = i\sigma_y K$ with $T_f^2 = -\underline{I}$ is the fermionic TR operator for electrons[18]. Therefore, the Kramers degeneracy does not hold in a general photonic system, unless other symmetry such as polarization degeneracy[15,21] or spatial symmetry[20] has been imposed in the system.

In another aspect, the combined Hamiltonian of the hybrid modes for Maxwell's equations with the degenerate condition: $\underline{\varepsilon} = -\underline{\mu}$ (at the reference frequency ω_0) is TR invariant under T_p, that is,

$$T_p \mathcal{H}_c T_p^{-1} = \mathcal{H}_c, \ \mathcal{H}_c = \begin{pmatrix} \mathcal{H}_+ & 0 \\ 0 & \mathcal{H}_- \end{pmatrix}, \tag{13}$$

where T_p is the fermionic-like *pseudo* TR operator having the same form of T_f. The pseudo TR operator T_p is inspired by noticing that $\mathbf{E}+\mathbf{H}' \leftrightarrow \mathbf{E}-\mathbf{H}'$ during the TR operation. The pseudo TR operator is thus defined as $T_p = T_b\sigma_x = \sigma_z K\sigma_x = i\sigma_y K$ with $T_p^2 = -\underline{I}$[21]. Here, $\sigma_x = (0, 1; 1, 0)$, $\sigma_y = (0, -i; i, 0)$, and $\sigma_z = \mathrm{diag}(1, -1)$ are the Pauli matrices. The pseudo TR symmetry of the combined Hamiltonian $\mathcal{H}_c$ ensures the Kramers degeneracy and guarantees the appearance of a Kramers doublet.

As revealed in Eq. (11), the photonic Kramers doublet consists of an eigenstate ψ_σ of $\mathcal{H}_+$ and another eigenstate $\psi_{-\sigma}$ of $\mathcal{H}_-$, with the same eigenvalue λ_σ ($\sigma = \pm 1$). The states ψ_σ and $\psi_{-\sigma}$ become TR partners under T_p, that is, $T_p\psi_\sigma = \psi_{-\sigma}^*$ and $T_p\psi_{-\sigma} = -\psi_\sigma^*$. In addition, ψ_σ and $\psi_{-\sigma}$ are orthogonal: $\langle\psi_\sigma|\psi_{-\sigma}\rangle = 0$ [cf. Eq. (30) in Methods B], which implies that it is impossible to introduce any backscattering between the two states, unless the TR symmetry has been broken. The two states therefore counterpropagate toward opposite directions without backscattering, a typical feature of the helical edge states that appear in the QSH system. As indicated in the field basis ψ [cf. Eq. (4)], the photonic Kramers doublet is a pair of two pseudospin states for the hybrid modes, analogous to the spin-up and spin-down states in electronic systems. The nonzero Chern numbers C_σ associated with the eigenstate ψ_σ further assert that the helical edge states are topologically protected, their existence being guaranteed by the difference of topological invariants on two sides of the interface. As the topological invariants remain constant under arbitrary continuous deformations of the system, the topological properties of the isotropic medium will be preserved when a certian anisotropy is included in the medium. The exact calculation of topological invariants for the anisotropic medium may resort to the numerical integration of Berry curvatures[49].

Surface modes. Let the xz plane be the interface between a dielectric with the relative material parameters ε_d, μ_d and a uniaxially anisotropic medium characterized by ε_t, ε_z, μ_t, and μ_z. The characteristic equation of surface modes is formulated based on Maxwell's boundary conditions: the continuity of tangential electric and magnetic field components at the interface, which is given by (see Methods C)

$$\begin{aligned}(\varepsilon_t\mu_t - \varepsilon_d\mu_d)k_z^2(k_x^2 + k_z^2 - \varepsilon_t\mu_t k_0^2) - \varepsilon_t\mu_t k_0^2(k_y^{(1)}\varepsilon_t - k_y^{(4)}\varepsilon_d)(k_y^{(2)}\mu_t - k_y^{(3)}\mu_d)\\ +k_z^2[\varepsilon_t\mu_t(k_y^{(1)}k_y^{(2)} + k_y^{(3)}k_y^{(4)}) - (\varepsilon_t\mu_d k_y^{(1)}k_y^{(3)} + \varepsilon_d\mu_t k_y^{(2)}k_y^{(4)})] = 0,\end{aligned} \tag{14}$$

where $k_y^{(1)} = k_y^{(2)} = \sqrt{\varepsilon_d\mu_d k_0^2 - k_x^2 - k_z^2}$ are the normal (to interface) wave vector components in the dielectric, and $k_y^{(3)} = -\sqrt{\varepsilon_z\mu_t k_0^2 - k_x^2 - \frac{\varepsilon_z}{\varepsilon_t}k_z^2}$ and $k_y^{(4)} = -\sqrt{\varepsilon_t\mu_z k_0^2 - k_x^2 - \frac{\mu_z}{\mu_t}k_z^2}$ are the normal components in the anisotropic medium. For the surface waves to be valid on the dielectric side ($y>0$), $k_y^{(1)}$ and $k_y^{(2)}$ should be purely imaginary with a positive value, which requires that $k_x^2 + k_z^2 > \varepsilon_d\mu_d k_0^2$. On the anisotropic medium side ($y<0$), $k_y^{(3)}$ and $k_y^{(4)}$ should be purely imaginary with a negative value, which requires that $k_x^2 + \frac{\varepsilon_z}{\varepsilon_t}k_z^2 > \varepsilon_z\mu_t k_0^2$ and $k_x^2 + \frac{\mu_z}{\mu_t}k_z^2 > \varepsilon_t\mu_z k_0^2$. In the presence of square roots in $k_y^{(n)}$ ($n = 1, 2, 3, 4$), the surface modes are represented by a part of the bi-quadratic surface in the frequency-wave vector space. In the isotropic case, where $\varepsilon_t = \varepsilon_z \equiv \varepsilon$ and $\mu_t = \mu_z \equiv \mu$, Eq. (14) is simplified to

$$k_x^2 + k_z^2 = \frac{\varepsilon\varepsilon_d(\varepsilon\mu_d - \mu\varepsilon_d)}{\varepsilon^2 - \varepsilon_d^2}k_0^2 \text{ or } k_x^2 + k_z^2 = \frac{\mu\mu_d(\mu\varepsilon_d - \varepsilon\mu_d)}{\mu^2 - \mu_d^2}k_0^2, \tag{15}$$

depending on whether $\varepsilon(\omega_0) < 0$ or $\mu(\omega_0) < 0$, respectively. In this situation, the characteristic equation represents a quadratic surface of revolution about the frequency axis.

At the reference frequency ω_0, where $\varepsilon_t = -\mu_t$ and $\varepsilon_z = -\mu_z$, Eq. (14) is reduced to

$$\begin{aligned}(\mu_t^2 - \varepsilon_d\mu_d)k_x^2 + (\mu_t\mu_z - \varepsilon_d\mu_d)k_z^2 - \varepsilon_d\mu_d\mu_t(\mu_t + \mu_z)k_0^2\\ +\mu_t(\varepsilon_d - \mu_d)\sqrt{k_x^2 + k_z^2 - \varepsilon_d\mu_d k_0^2}\sqrt{k_x^2 + \frac{\mu_z}{\mu_t}k_z^2 + \mu_z\mu_t k_0^2} = 0,\end{aligned} \tag{16}$$

which is a part of the bi-quadratic curve. If $\varepsilon_d = \mu_d$, Eq. (16) is further simplified to a standard quadratic curve as

$$(\mu_t^2 - \mu_d^2)k_x^2 + (\mu_t\mu_z - \mu_d^2)k_z^2 = \mu_d^2\mu_t(\mu_t + \mu_z)k_0^2, \tag{17}$$

which represents an ellipse when $\mu_t^2 > \mu_d^2$ and $\mu_t\mu_z > \mu_d^2$ or a two-sheeted hyperbola when $\mu_t\mu_z < \mu_d^2 < \mu_t^2$ or $\mu_t^2 < \mu_d^2 < \mu_t\mu_z$. Here, we assume that μ_t and μ_z are of the same sign. In the isotropic case, Eq. (15) at the reference frequency ω_0 is simplified to

$$k_x^2 + k_z^2 = \frac{\varepsilon^2\varepsilon_d(\varepsilon_d + \mu_d)}{\varepsilon^2 - \varepsilon_d^2}k_0^2 \text{ or } k_x^2 + k_z^2 = \frac{\mu^2\mu_d(\varepsilon_d + \mu_d)}{\mu^2 - \mu_d^2}k_0^2, \tag{18}$$

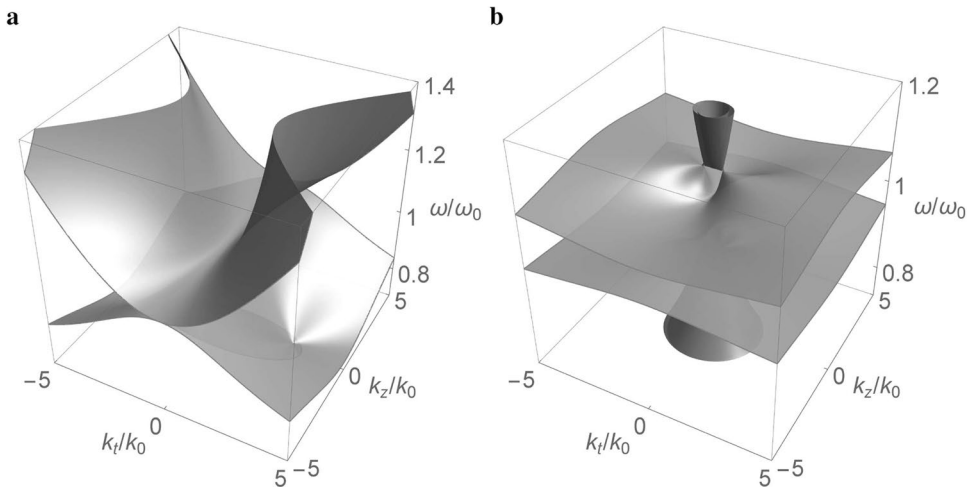

Figure 1. Dispersion of bulk modes in the frequency-wave vector space for the dispersive metamaterial based on Eq. (2) with $\omega_p/\omega_0 = 1.5$ and (**a**) $\varepsilon_{t\infty} = 0.25$, $\mu_{t\infty} = 4.25$, $\varepsilon_{z\infty} = \mu_{z\infty} = 2.25$ ($\varepsilon_t = -\mu_t = -2$, $\varepsilon_z = \mu_z = 0$ at $\omega = \omega_0$) (**b**) $\varepsilon_{t\infty} = 1.9$, $\varepsilon_{z\infty} = 2.1$, $\mu_{t\infty} = 2.6$, $\mu_{z\infty} = 2.4$ ($\varepsilon_t = -\mu_t = -0.35$, $\varepsilon_z = -\mu_z = -0.15$ at $\omega = \omega_0$).

depending on whether $\varepsilon < 0$ or $\mu < 0$, respectively. In this situation, the characteristic equation represents a circle when $\varepsilon^2 > \varepsilon_d^2$ or $\mu^2 > \varepsilon_d^2$, which is valid even when $\varepsilon_d \neq \mu_d$. In case all the materials considered are non-magnetic, that is, $\mu = 1$ ($\varepsilon = -1$) and $\mu_d = 1$ at $\omega = \omega_0$, Eq. (16) is simplified to $k_x^2 + k_z^2 = \varepsilon_d k_0^2/(1 - \varepsilon_d)$, which represents a circle when $0 < \varepsilon_d < 1$.

For a fixed k_z (k_x), Eq. (16) allows for two solutions of k_x (k_z) with reflection symmetry about the k_z (k_x) axis, which means that there exist a pair of surface modes at the interface counterpropagating toward the positive and negative k_x (k_z) directions.

Discussion

Figure 1 shows the dispersion of bulk modes in the frequency-wave vector space for the dispersive medium based on Eq. (2). The Drude-type dispersive model, which is usually employed in the analysis of metamaterials, is assumed for the permittivity and permeability components: $\varepsilon_n = \varepsilon_{n\infty} - \omega_{ep}^2/\omega^2$ and $\mu_n = \mu_{n\infty} - \omega_{mp}^2/\omega^2$ ($n = t, z$)[50,51], where ω_{ep} and ω_{mp} are the effective plasma frequency and magnetic plasma frequency, respectively[52,53]. For simplicity, we further assume that $\omega_{ep} = \omega_{mp} \equiv \omega_p$[50,51]. If $\varepsilon_z = 0$ or $\varepsilon_t = 0$ at the reference frequency ω_0, the upper and the lower modes touch at $\omega = \omega_0$ [Fig. 1(a)]. In particular, the upper mode has a positive index (along the optical axis): $n_z \equiv \sqrt{\varepsilon_z \mu_z} > 0$, while the lower mode has a negative index: $n_z < 0$.

If both $\varepsilon_t \neq 0$ and $\varepsilon_z \neq 0$ at $\omega = \omega_0$, a frequency gap is opened between the two bulk modes, with the gap size dependent on the material parameters [Fig. 1(b)]. As the anisotropy of the medium is reduced, the bulk modes tend to be dispersionless, that is, independent of the frequency. In the isotropic case, where $\varepsilon_{t\infty} = \varepsilon_{z\infty} \equiv \varepsilon_\infty$ and $\mu_{t\infty} = \mu_{z\infty} \equiv \mu_\infty$, the bulk modes are basically represented by two flat surfaces at $\omega = \omega_p/\sqrt{\varepsilon_\infty}$ and $\omega = \omega_p/\sqrt{\mu_\infty}$, leaving in between a frequency gap when $\varepsilon_\infty \neq \mu_\infty$.

Figure 2(a) shows the dispersion of surface mode (in red color) at the interface between vacuum and the dispersive metamaterial based on Eq. (14), which exists in the frequency gap between two bulk modes (in gray color). The surface mode is represented by a funnel-shaped surface with a lower frequency at the center that connects to the lower bulk mode. As k_x or k_z increases, the surface mode raises its frequency and approaches asymptotically to

$$\omega_{sx} = \frac{\omega_p}{\sqrt{\varepsilon_d + \varepsilon_{t\infty}}} \text{ or } \omega_{sz} = \omega_p \sqrt{\frac{(\sqrt{(\varepsilon_{t\infty} - \varepsilon_{z\infty})^2 + 4\varepsilon_d^2} - \varepsilon_{t\infty} - \varepsilon_{z\infty})}{2(\varepsilon_d^2 - \varepsilon_{t\infty}\varepsilon_{z\infty})}}, \tag{19}$$

respectively, which are obtained by taking the limit as $k_x \to \infty$ or $k_z \to \infty$ in the characteristic equation of surface mode [cf. Eq. (14)]. There may exist a gap between the surface mode and the upper bulk mode, depending on the constitutive parameters of the metamaterial. For $\varepsilon_{z\infty} > \varepsilon_{t\infty}$ ($\varepsilon_{z\infty} < \varepsilon_{t\infty}$), the lowest frequency of the upper bulk mode is given by $\omega_b = \omega_p/\sqrt{\varepsilon_{z\infty}}$ ($\omega_b = \omega_p/\sqrt{\varepsilon_{t\infty}}$). A gap is opened when $\omega_b > \omega_{sx}$ ($\omega_b > \omega_{sz}$), where we also have $\omega_{sz} < \omega_{sx}$ ($\omega_{sx} < \omega_{sz}$). At the reference frequency ω_0, where the degenerate condition $\varepsilon = -\mu$ is satisfied, the surface mode is described by an ellipse (denoted by black curve) with $\varepsilon_d = \mu_d$ and $\mu_t^2 > \mu_t \mu_z > \mu_d^2$ [cf. Eq. (17)]. In the isotropic case where $\varepsilon_{t\infty} = \varepsilon_{z\infty} = \varepsilon_\infty$, the surface mode approaches asymptotically to a flat surface for a sufficiently large k_x or k_z, as shown in Fig. 2(b). The asymptotic frequency becomes $\omega_s = \omega_p/\sqrt{\varepsilon_d + \varepsilon_\infty}$ [cf. Eq. (19)], which has the same form of the surface plasma frequency at the interface between a dielectric and the Drude-type metal. In this situation, there is always a gap between the surface mode and the upper bulk mode. At the reference frequency ω_0, the surface mode is represented by a circle [cf. Eq. (18)].

Since the surface waves are evanescent in the direction normal to the interface, their normal wave vector components are purely imaginary, that is, $k_y = \pm i\kappa_y$ and κ_y is real. The transversality condition ($k \cdot E = 0$) dictates that

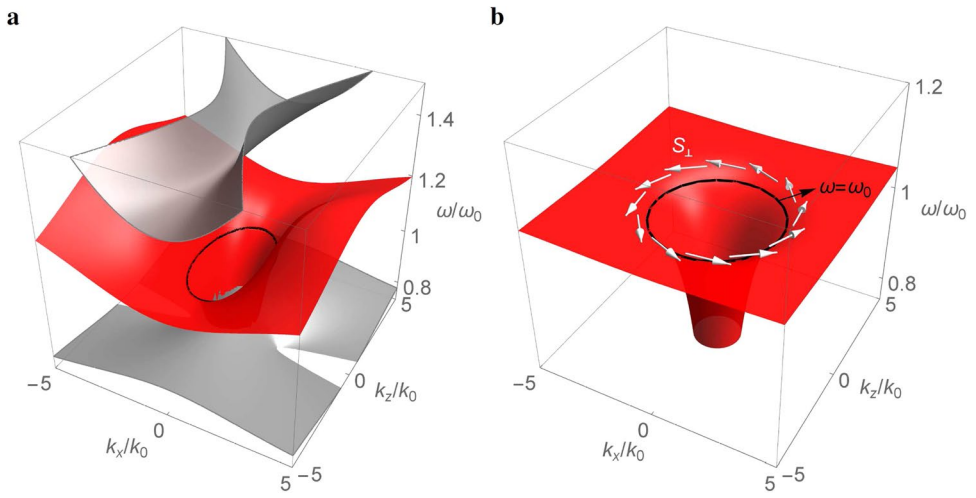

Figure 2. Dispersion of surface modes (in red color) at the interface between vacuum and the dispersive metamaterial based on Eq. (14) with $\omega_p/\omega_0 = 1.5$ and (**a**) $\varepsilon_{t\infty} = 0.25$, $\varepsilon_{z\infty} = 1.25$, $\mu_{t\infty} = 4.25$, $\mu_{z\infty} = 3.25$ ($\varepsilon_t = -\mu_t = -2$ and $\varepsilon_z = -\mu_z = -1$ at $\omega = \omega_0$) and (**b**) $\varepsilon_{t\infty} = \varepsilon_{z\infty} = 1.05$ and $\mu_{t\infty} = \mu_{z\infty} = 3.45$ ($\varepsilon_t = \varepsilon_z = -\mu_t = -\mu_z = -1.2$ at $\omega = \omega_0$). Black curves are surface modes at $\omega = \omega_0$. Gray surfaces in (**a**) are bulk modes. White arrows in (**b**) denote the transverse spin $\mathbf{S}_\perp$.

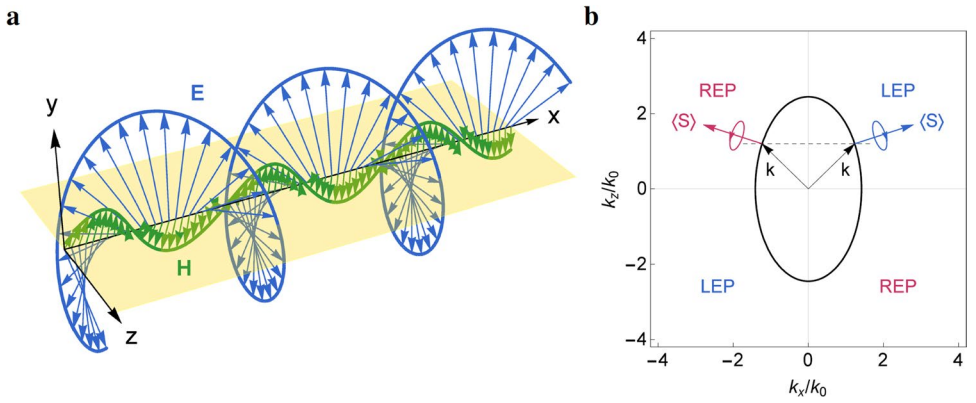

Figure 3. (**a**) Instantaneous electric field $\mathbf{E}(\mathbf{r}, t) = \mathrm{Re}[\mathbf{E}(\mathbf{r})e^{-i\omega t}]$ and magnetic field $\mathbf{H}(\mathbf{r}, t) = \mathrm{Re}[\mathbf{H}(\mathbf{r})e^{-i\omega t}]$ for the surface wave at the interface between vacuum ($y > 0$) and the dispersive metamaterial ($y < 0$) at the reference frequency ω_0 with the same parameters in Fig. 2(a). Light yellow plane denotes the interface. (**b**) Polarization handedness of the same surface wave for different signs of k_x and k_z. Black dashed line indicates the constant $k_z = 1.2k_0$. Black arrows are wave vectors. Blue and red arrows denote the energy flows for $k_x > 0$ and $k_x < 0$, respectively.

the normal (to interface) electric field component E_y has a $\pi/2$ phase difference relative to the tangential component E_x or E_z. As the wave propagates at the interface ($y = 0$), the electric fields rotate in the perpendicular (xy or yz) plane, leading to elliptically polarized waves. The elliptical polarization of the surface waves is demonstrated in Fig. 3(a), where the instantaneous electric fields (blue arrows) and magnetic fields (green arrows) at the interface result in helical trajectories (traced by the tips of field vectors) along the propagation direction (the helical trajectory for the magnetic fields is less obvious as the normal magnetic field componet H_y is relatively smaller than the electric field component E_y). In particular, the rotating electric field generates a *transverse spin* $\mathbf{S}_\perp$ perpendicular to the wave vector $\mathbf{k}$ as[54]

$$\mathbf{S}_\perp = \frac{\mathrm{Re}[\mathbf{k}] \times \mathrm{Im}[\mathbf{k}]}{(\mathrm{Re}[\mathbf{k}])^2}, \tag{20}$$

which is considered as the spin-momentum locking in the evanescent surface waves. The transverse spin of the surface mode exhibits a vortex spin texture [denoted by white arrows in Fig. 2(b)] that occurs in the surface states for 3D topological insulators.

For the evanescent surface wave with the transverse spin, the handedness can be evaluated by first calculating the electric field components in a new coordinate system (x', y', z'), obtained by rotating the original system (x, y, z)

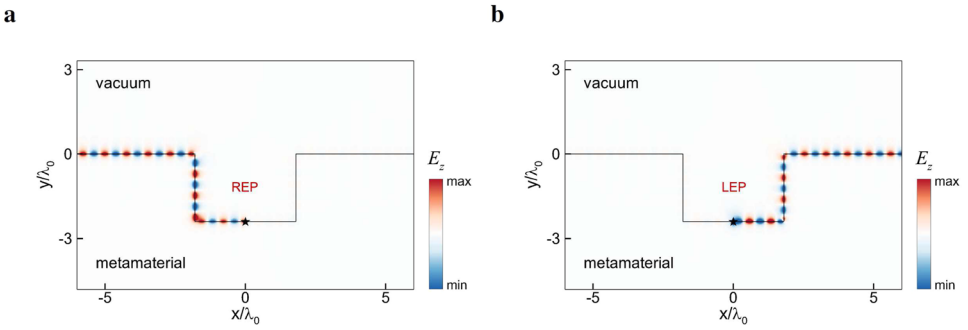

Figure 4. Electromagnetic wave simulation for the surface modes at the interface between vacuum and the dispersive metamaterial with the same paramsters in Fig. 3(b). Asteristic symbols denote the dipole sources for exciting the (**a**) REP and (**b**) LEP surface waves at the reference frequency ω_0.

about the y axis such that the x' axis is oriented to the time-averaged Poynting vector on the xz plane. Denoting θ the angle from the x axis to the x' axis, the electric field components in the new coordinate system are given by $E_{x'} = E_x\cos\theta + E_z\sin\theta$, $E_{y'} = E_y$, and $E_{z'} = -E_x\sin\theta + E_z\cos\theta$. The polarization handedness is then determined by the phase difference δ between $E_{y'}$ and $E_{z'}$: $\delta = arg(E_{z'}) - arg(E_{y'})$, where $arg(z) \equiv arctan(\mathrm{Im}[z]/\mathrm{Re}[z])$ is the argument of a complex number z. The wave is right-handed elliptically polarized (REP) or left-handed elliptically polarized (LEP) if $\delta = \pi/2$ or $-\pi/2$, respectively, that is, the phase of $E_{z'}$ is delayed or advanced by 90° relative to that of $E_{y'}$ (under the time-harmonic convention $e^{-i\omega t}$).

In Fig. 3(b), the polarization handedness of the surface waves at the reference frequency ω_0 is shown to have odd symmetry with respect to either of the two in-plane wave vector components (k_x and k_z). For a constant k_z (indicated by black dashed line), there exist a LEP wave propagating toward the positive k_x direction and a REP wave toward the negative k_x direction. The two surface waves with opposite handedness counterpropagate at a given edge ($y = 0$ in the xy plane), showing the feature of spin-momentum locking that occurs in the helical edge states. This feature holds when the surface mode is described by either an ellipse (for the anisotropic medium) or a circle (for the isotropic medium).

Finally, the topological properties of the surface modes are illustrated with the electromagnetic wave propagation at the interface between vacuum and the metamaterial[55], as shown in Fig. 4. Here, a dipole source with $k_z/k_0 = 1.2$ is placed at the interface (marked by asterisk symbol) to excite the surface wave, where the field is evanescent both in vacuum (outside the dispersion circle: $k_x^2 + k_z^2 > k_0^2$) and the metamaterial (inside the frequency gap). By appropriately adjusting the phase of the point dipole, the REP (LEP) surface wave at the reference frequency ω_0 propagates unidirectionally toward the left (right), which is consistent with the direction of surface wave energy flow [cf. Figure 3(b)] and exhibits the typical feature of spin-polarized helical edge states. In particular, the surface waves are able to bend around sharp corners without backscattering, showing the robust transport of edge states against disorder. As the frequency deviates from ω_0, the degenerate condition ($\varepsilon = -\mu$) will be violated to a certain extent. The removal of degeneracy, however, is tolerated to some degree for the system to remain in the photonic topological phase[15,23].

In conclusion, we have analyzed the photonic topological phases in dispersive metamaterials with the degenerate condition at a reference frequency. The topological phases are characterized by the nonzero spin Chern numbers for the hybrid modes described by the spin-orbit Hamiltonians with pseudospin 1. In particular, the hybrid modes comply with a fermionic-like pseudo TR symmetry that ensures the Kramers degeneracy, leading to the topological protection of helical edge states. The transverse spin generated by the evanescent surface wave is perpendicular to the wave vector, which exhibits the spin-momentum locking as in the surface states for 3D topological insulators. The topological features of helical edge states are further demonstrated by the robust transport of surface waves at an irregular boundary between vacuum and the dispersive metamaterial.

Methods

Spin-orbit Hamiltonians. The wave equation for the plus hybrid mode $\mathbf{F} = \mathbf{E} + \mathbf{H}'$ in Eq. (3) can be rewritten as

$$\mathcal{H}_+\widetilde{\psi} = \widetilde{D}\widetilde{\psi}, \tag{21}$$

where

$$\mathcal{H}_+ = c\begin{pmatrix} \kappa_z & \frac{\kappa_x - i\kappa_y}{\sqrt{2}} & 0 \\ \frac{\kappa_x + i\kappa_y}{\sqrt{2}} & 0 & \frac{\kappa_x - i\kappa_y}{\sqrt{2}} \\ 0 & \frac{\kappa_x + i\kappa_y}{\sqrt{2}} & -\kappa_z \end{pmatrix}, \quad \widetilde{D} = \omega\begin{pmatrix} \varepsilon_t & 0 & 0 \\ 0 & \varepsilon_z & 0 \\ 0 & 0 & \varepsilon_t \end{pmatrix}, \tag{22}$$

and $\widetilde{\psi} = \left(\frac{-F_x + iF_y}{\sqrt{2}}, F_z, \frac{F_x + iF_y}{\sqrt{2}}\right)^T$ is the basis of the *pseudospin* states that include a $\pi/2$ phase difference in the transverse field components (with respect to the optical axis of the anisotropic medium)[45]. In the neighborhood of ω_0, ε_n is approximated as $\omega\varepsilon_n \approx \omega_0\varepsilon_{n0} + \widetilde{\varepsilon}_n\delta\omega$ $(n = t, z)$ and Eq. (21) can be rearranged as

$$\mathcal{H}_+\psi - D\psi = \delta\omega\psi, \tag{23}$$

where

$$\mathcal{H}_+ = \frac{c}{\sqrt{\widetilde{\varepsilon}_t\widetilde{\varepsilon}_z}}\begin{pmatrix} \sqrt{\frac{\widetilde{\varepsilon}_z}{\widetilde{\varepsilon}_t}}\kappa_z & \frac{\kappa_x - i\kappa_y}{\sqrt{2}} & 0 \\ \frac{\kappa_x + i\kappa_y}{\sqrt{2}} & 0 & \frac{\kappa_x - i\kappa_y}{\sqrt{2}} \\ 0 & \frac{\kappa_x + i\kappa_y}{\sqrt{2}} & -\sqrt{\frac{\widetilde{\varepsilon}_z}{\widetilde{\varepsilon}_t}}\kappa_z \end{pmatrix}, \quad D = \omega_0\begin{pmatrix} \frac{\varepsilon_{t0}}{\widetilde{\varepsilon}_t} & 0 & 0 \\ 0 & \frac{\varepsilon_{t0}}{\widetilde{\varepsilon}_z} & 0 \\ 0 & 0 & \frac{\varepsilon_{t0}}{\widetilde{\varepsilon}_t} \end{pmatrix}, \tag{24}$$

and $\psi = U^{-1}\widetilde{\psi}$ with $U = \mathrm{diag}(\sqrt{\widetilde{\varepsilon}_z/\widetilde{\varepsilon}_t}, 1, \sqrt{\widetilde{\varepsilon}_z/\widetilde{\varepsilon}_t})$. In the isotropic case, where $\varepsilon_{t0} = \varepsilon_{z0} \equiv \varepsilon$ and $\widetilde{\varepsilon}_t = \widetilde{\varepsilon}_z \equiv \widetilde{\varepsilon}$, Eq. (23) is simplified to

$$\mathcal{H}_+\psi - d\psi = \delta\omega\psi, \tag{25}$$

where $d = \omega_0\varepsilon/\widetilde{\varepsilon}$ and

$$\mathcal{H}_+ = \alpha S \cdot \kappa, \tag{26}$$

with $\alpha = c/\widetilde{\varepsilon}$, $\kappa = \kappa_x\hat{x} + \kappa_y\hat{y} + \kappa_z\hat{z}$, $\mathbf{S} = S_x\hat{x} + S_y\hat{y} + S_z\hat{z}$, and

$$S_x = \frac{1}{\sqrt{2}}\begin{pmatrix} 0 & 1 & 0 \\ 1 & 0 & 1 \\ 0 & 1 & 0 \end{pmatrix}, \quad S_y = \frac{1}{\sqrt{2}}\begin{pmatrix} 0 & -i & 0 \\ i & 0 & -i \\ 0 & i & 0 \end{pmatrix}, \quad S_z = \begin{pmatrix} 1 & 0 & 0 \\ 0 & 0 & 0 \\ 0 & 0 & -1 \end{pmatrix} \tag{27}$$

being the spin matrices for spin 1.

Topological invariants. In terms of spherical coordinates, the Hamiltonian for the plus hybrid mode $\mathcal{H}_+ = \alpha S \cdot \kappa$ [cf. Eq. (26)] can be rewritten as

$$\mathcal{H}_+ = \frac{|d|}{\sqrt{2}}\begin{pmatrix} \sqrt{2}\cos\theta & \sin\theta e^{-i\phi} & 0 \\ \sin\theta e^{i\phi} & 0 & \sin\theta e^{-i\phi} \\ 0 & \sin\theta e^{i\phi} & -\sqrt{2}\cos\theta \end{pmatrix}, \tag{28}$$

where $\kappa_x = a\sin\theta\cos\phi$, $\kappa_y = a\sin\theta\sin\phi$, and $\kappa_z = a\cos\theta$ with $a = |\varepsilon k_0|$. Here, θ and ϕ are the polar angle and azimuthal angle, respectively, on the closed surface S: $\kappa_x^2 + \kappa_y^2 + \kappa_z^2 = \varepsilon^2 k_0^2$, corresponding to the bulk mode at the reference frequency ω_0 in the imaginary wave vector space. The eigensystem of the plus hybrid mode

$$\mathcal{H}_+\psi_\sigma = \lambda_\sigma\psi_\sigma, \tag{29}$$

is solved to give the eigenvalues $\lambda_\sigma = |d|\sigma$ $(\sigma = \pm 1, 0)$ and the normalized eigenvectors as

$$\psi_\sigma = \frac{1}{2}\begin{pmatrix} \sigma e^{-2i\phi}(\sigma + \cos\theta) \\ \sigma\sqrt{2}e^{-i\phi}\sin\theta \\ 1 - \sigma\cos\theta \end{pmatrix} (\sigma = \pm 1), \tag{30}$$

$$\psi_\sigma = \frac{1}{\sqrt{2}}\begin{pmatrix} -e^{-2i\phi}\sin\theta \\ \sqrt{2}e^{-i\phi}\cos\theta \\ \sin\theta \end{pmatrix} (\sigma = 0). \tag{31}$$

Note here that the eigenvalue λ_σ is related to $\delta\omega$ in Eq. (4) as $\lambda_\sigma = d + \delta\omega$, while the eigenfuntion ψ_σ is the same as ψ. Based on Eqs (30) and (31), the Berry connections $\mathbf{A}_\sigma = -i\langle\psi_\sigma|\nabla\psi_\sigma\rangle$ are obtained as

$$\mathbf{A}_\sigma = -\frac{1}{r}\cot\frac{\theta}{2}\hat{\phi} \quad (\sigma = 1), \tag{32}$$

$$\mathbf{A}_\sigma = -\frac{1}{r}\tan\frac{\theta}{2}\hat{\phi} \quad (\sigma = -1), \tag{33}$$

$$\mathbf{A}_\sigma = -\frac{1}{r}\csc\ \theta\hat{\phi} \quad (\sigma = 0). \tag{34}$$

The Berry curvatures $\mathbf{F}_\sigma = \nabla \times \mathbf{A}_\sigma$ are thus given by

$$\mathbf{F}_\sigma = \sigma\frac{\hat{r}}{r^2} \quad (\sigma = \pm 1,\ 0). \tag{35}$$

Integrating over the closed sphere S, the Chern numbers $C_\sigma = \frac{1}{2\pi}\int_S \mathbf{F}_\sigma \cdot d\mathbf{s}$ are calculated to give

$$C_\sigma = 2\sigma \quad (\sigma = \pm 1,\ 0). \tag{36}$$

Surface wave equation. According to Maxwell's equations, the eigenfields on either side of the interface ($y = 0$) are given by the nontrivial solutions of E and H [cf. Eq. (1)] or the *null space* of H_m [cf. Eq. (12)]. On the dielectric side ($y > 0$), we have

$$\mathbf{H}^{(1)} = \frac{1}{k_0\eta_0}(k_z,\ \ 0,\ -k_x), \quad \mathbf{E}^{(1)} = \frac{1}{k_0^2\varepsilon_d}\left(k_x k_y^{(1)},\ -k_x^2 - k_z^2,\ k_y^{(1)}k_z\right), \tag{37}$$

$$\mathbf{H}^{(2)} = \frac{1}{k_0\eta_0}(k_y^{(2)},\ -k_x, 0),\ \mathbf{E}^{(2)} = -\frac{1}{k_0^2\varepsilon_d}\left(k_x k_z,\ k_y^{(2)}k_z,\ k_z^2 - \varepsilon_d\mu_d\right), \tag{38}$$

where $k_y^{(1)} = k_y^{(2)} = \sqrt{\varepsilon_d\mu_d k_0^2 - k_x^2 - k_z^2}$ are the normal (to interface) wave vector components, and the superscripts (1) and (2) refer to two independent polarizations in the dielectric. On the anisotropic medium side ($y < 0$), the eigenfields are given by

$$\mathbf{H}^{(3)} = \frac{1}{k_0\eta_0}(k_y^{(3)},\ -k_x,\ 0),\ \mathbf{E}^{(3)} = -\frac{1}{k_0^2\varepsilon_t}\left(k_x k_z,\ k_y^{(3)}k_z,\ k_z^2 - \varepsilon_t\mu_t\right), \tag{39}$$

$$\mathbf{H}^{(4)} = \frac{1}{k_0^2\eta_0}\left(k_x k_z,\ k_y^{(4)}k_z,\ k_z^2 - \varepsilon_t\mu_t\right),\ \mathbf{E}^{(4)} = \frac{\mu_t}{k_0}\left(k_y^{(4)},\ -k_x,\ 0\right), \tag{40}$$

where $k_y^{(3)} = -\sqrt{\varepsilon_z\mu_t k_0^2 - k_x^2 - \frac{\varepsilon_z}{\varepsilon_t}k_z^2}$ and $k_y^{(4)} = -\sqrt{\varepsilon_t\mu_z k_0^2 - k_x^2 - \frac{\mu_z}{\mu_t}k_z^2}$, and the superscripts (3) and (4) refer to two independent polarizations in the anisotropic medium. Note that the eigenfields in Eqs (37)–(40) share the common tangential wave vector components k_x and k_z across the interface, as a direct consequence of the phase matching of electromagnetic fields.

According to Maxwell's boundary conditions, the tangential electric and magnetic field components are continuous at the interface:

$$C_1H_{x,z}^{(1)} + C_2H_{x,z}^{(2)} = C_3H_{x,z}^{(3)} + C_4H_{x,z}^{(4)}, \tag{41}$$

$$C_1E_{x,z}^{(1)} + C_2E_{x,z}^{(2)} = C_3E_{x,z}^{(3)} + C_4E_{x,z}^{(4)}, \tag{42}$$

where C_1, C_2, C_3, and C_4 are constants. The existence of a nontrivial solution of these constants requires that the determinant of the 4×4 matrix obtained from Eqs (41) and (42) be zero, which gives the characteristic equation of the surface mode as

$$\begin{aligned}&(\varepsilon_t\mu_t - \varepsilon_d\mu_d)k_z^2(k_x^2 + k_z^2 - \varepsilon_t\mu_t k_0^2) - \varepsilon_t\mu_t k_0^2(k_y^{(1)}\varepsilon_t - k_y^{(4)}\varepsilon_d)(k_y^{(2)}\mu_t - k_y^{(3)}\mu_d)\\ &+k_z^2[\varepsilon_t\mu_t(k_y^{(1)}k_y^{(2)} + k_y^{(3)}k_y^{(4)}) - (\varepsilon_t\mu_d k_y^{(1)}k_y^{(3)} + \varepsilon_d\mu_t k_y^{(2)}k_y^{(4)})] = 0.\end{aligned} \tag{43}$$

Simulation. The simulation domain is on the x-y plane and k_z is the out-of-plane wave vector component, which is kept fixed in the simulation so that the eigenwaves possess the same k_z[55]. The surface mode is excited by a dipole source placed at the boundary of the metamaterial, which can be implemented by a dipole antenna in the experiments[10,17,35,38]. For the dipole to serve as the source of circular or elliptical polarization, the dipole has two in-plane components and the phase difference in between is set to be $\pi/2$ or $-\pi/2$ to mimic the right-handed or left-handed wave[36].

References

1. Fu, L., Kane, C. L. & Mele, E. J. Topological insulators in three dimensions. *Phys. Rev. Lett.* **98**, 106803 (2007).
2. Fu, L. & Kane, C. L. Topological insulators with inversion symmetry. *Phys. Rev. B* **76**, 045302 (2007).
3. Moore, J. E. & Balents, L. Topological invariants of time-reversal-invariant band structures. *Phys. Rev. B* **75**, 121306 (2007).
4. Qi, X.-L., Hughes, T. L. & Zhang, S.-C. Topological field theory of time-reversal invariant insulators. *Phys. Rev. B* **78**, 195424 (2008).
5. Roy, R. Z_2 classification of quantum spin Hall systems: an approach using time-reversal invariance. *Phys. Rev. B* **79**, 195321 (2009).
6. Hasan, M. Z. & Kane, C. L. Colloquium: topological insulators. *Rev. Mod. Phys.* **82**, 3045–3067 (2010).

7. Qi, X.-L. & Zhang, S.-C. Topological insulators and superconductors. *Rev. Mod. Phys.* **83**, 1057–1110 (2011).
8. Haldane, F. D. M. & Raghu, S. Possible realization of directional optical waveguides in photonic crystals with broken time-reversal symmetry. *Phys. Rev. Lett.* **100**, 013904 (2008).
9. Wang, Z., Chong, Y. D., Joannopoulos, J. D. & Soljačić, M. Reflection-free one-way edge modes in a gyromagnetic photonic crystal. *Phys. Rev. Lett.* **100**, 013905 (2008).
10. Wang, Z., Chong, Y., Joannopoulos, J. D. & Soljačić, M. Observation of unidirectional backscattering-immune topological electromagnetic states. *Nature* **461**, 772–775 (2009).
11. Hafezi, M., Demler, E. A., Lukin, M. D. & Taylor, J. M. Robust optical delay lines with topological protection. *Nat. Phys.* **7**, 907–912 (2011).
12. Fang, K., Yu, Z. & Fan, S. Realizing effective magnetic field for photons by controlling the phase of dynamic modulation. *Nat. Photonics* **6**, 782–787 (2012).
13. Hafezi, M., Mittal, S., Fan, J., Migdall, A. & Taylor, J. Imaging topological edge states in silicon photonics. *Nat. Photonics* **7**, 1001–1005 (2013).
14. Rechtsman, M. C. *et al*. Photonic Floquet topological insulators. *Nature* **496**, 196–200 (2013).
15. Khanikaev, A. B. *et al*. Photonic topological insulators. *Nat. Mater.* **12**, 233–239 (2013).
16. Liang, G. Q. & Chong, Y. D. Optical resonator analog of a two-dimensional topological insulator. *Phys. Rev. Lett.* **110**, 203904 (2013).
17. Chen, W.-J. *et al*. Experimental realization of photonic topological insulator in a uniaxial metacrystal waveguide. *Nat. Commun.* **5**, 5782 (2014).
18. Lu, L., Joannopoulos, J. D. & Soljačić, M. Topological photonics. *Nat. Photonics* **8**, 821–829 (2014).
19. Ma, T., Khanikaev, A. B., Mousavi, S. H. & Shvets, G. Guiding electromagnetic waves around sharp corners: topologically protected photonic transport in metawaveguides. *Phys. Rev. Lett.* **114**, 127401 (2015).
20. Wu, L.-H. & Hu, X. Scheme for achieving a topological photonic crystal by using dielectric material. *Phys. Rev. Lett.* **114**, 223901 (2015).
21. He, C. *et al*. Photonic topological insulator with broken time-reversal symmetry. *Proc. Natl. Acad. Sci. USA* **113**, 4924–4928 (2016).
22. Silveirinha, M. G. Z2 topological index for continuous photonic materials. *Phys. Rev. B* **93**, 075110 (2016).
23. Slobozhanyuk, A. *et al*. Three-dimensional all-dielectric photonic topological insulator. *Nat. Photonics* **11**, 130–136 (2017).
24. Kosterlitz, J. M. & Thouless, D. J. Ordering, metastability and phase transitions in two-dimensional systems. *J. Phys. C: Solid State Phys.* **6**, 1181 (1973).
25. Klitzing, Kv, Dorda, G. & Pepper, M. New method for high-accuracy determination of the fine-structure constant based on quantized Hall resistance. *Phys. Rev. Lett.* **45**, 494–497 (1980).
26. Halperin, B. I. Quantized Hall conductance, current-carrying edge states, and the existence of extended states in a two-dimensional disordered potential. *Phys. Rev. B* **25**, 2185–2190 (1982).
27. Thouless, D. J., Kohmoto, M., Nightingale, M. P. & den Nijs, M. Quantized Hall conductance in a two-dimensional periodic potential. *Phys. Rev. Lett.* **49**, 405–408 (1982).
28. Kane, C. L. & Mele, E. J. Quantum spin Hall effect in graphene. *Phys. Rev. Lett.* **95**, 226801 (2005).
29. Bernevig, B. A. & Zhang, S.-C. Quantum spin Hall effect. *Phys. Rev. Lett.* **96**, 106802 (2006).
30. Bernevig, B. A., Hughes, T. L. & Zhang, S.-C. Quantum spin Hall effect and topological phase transition in HgTe quantum wells. *Science* **314**, 1757 (2006).
31. Wu, C., Bernevig, B. A. & Zhang, S.-C. Helical liquid and the edge of quantum spin Hall systems. *Phys. Rev. Lett.* **96**, 106401 (2006).
32. Kane, C. L. & Mele, E. J. Z2 topological order and the quantum spin Hall effect. *Phys. Rev. Lett.* **95**, 146802 (2005).
33. Sheng, D. N., Weng, Z. Y., Sheng, L. & Haldane, F. D. M. Quantum spin-Hall effect and topologically invariant Chern numbers. *Phys. Rev. Lett.* **97**, 036808 (2006).
34. Jacobs, D. A., Miroshnichenko, A. E., Kivshar, Y. S. & Khanikaev, A. B. Photonic topological Chern insulators based on Tellegen metacrystals. *New J. Phys.* **17**, 125015 (2015).
35. Slobozhanyuk, A. P. *et al*. Experimental demonstration of topological effects in bianisotropic metamaterials. *Sci. Rep.* **6**, 22270 (2016).
36. Dong, J.-W., Chen, X.-D., Zhu, H., Wang, Y. & Zhang, X. Valley photonic crystals for control of spin and topology. *Nat. Mater.* **16**, 298–302 (2017).
37. Chen, X.-D., Deng, W.-M., Lu, J.-C. & Dong, J.-W. Valley-controlled propagation of pseudospin states in bulk metacrystal waveguides. *Phys. Rev. B* **97**, 184201 (2018).
38. Cheng, X. *et al*. Robust reconfigurable electromagnetic pathways within a photonic topological insulator. *Nat. Mater.* **15**, 542–548 (2016).
39. Lai, K., Ma, T., Bo, X., Anlage, S. & Shvets, G. Experimental realization of a reflections-free compact delay line based on a photonic topological insulator. *Sci. Rep.* **6**, 28453 (2016).
40. Gao, F. *et al*. Topologically protected refraction of robust kink states in valley photonic crystals. *Nat. Phys.* **14**, 140 (2018).
41. Kang, Y., Ni, X., Cheng, X., Khanikaev, A. B. & Genack, A. Z. Pseudo-spin-valley coupled edge states in a photonic topological insulator. *Nat. Commun.* **9**, 3029 (2018).
42. Sabyasachi, B., Hirokazu, M., Wade, D., Edo, W. & Mohammad, H. Two-dimensionally confined topological edge states in photonic crystals. *New J. Phys.* **18**, 113013 (2016).
43. Xu, L., Wang, H.-X., Xu, Y.-D., Chen, H.-Y. & Jiang, J.-H. Accidental degeneracy in photonic bands and topological phase transitions in two-dimensional core-shell dielectric photonic crystals. *Opt. Express* **24**, 18059–18071 (2016).
44. Mei, J., Chen, Z. & Wu, Y. Pseudo-time-reversal symmetry and topological edge states in two-dimensional acoustic crystals. *Sci. Rep.* **6**, 32752 (2016).
45. Fang, A., Zhang, Z. Q., Louie, S. G. & Chan, C. T. Klein tunneling and supercollimation of pseudospin-1 electromagnetic waves. *Phys. Rev. B* **93** (2016).
46. Chen, W.-J., Zhang, Z.-Q., Dong, J.-W. & Chan, C. T. Symmetry-protected transport in a pseudospin-polarized waveguide. *Nat. Commun.* **6**, 8183 (2015).
47. Chen, X.-D., Deng, Z.-L., Chen, W.-J., Wang, J.-R. & Dong, J.-W. Manipulating pseudospin-polarized state of light in dispersion-immune photonic topological metacrystals. *Phys. Rev. B* **92**, 014210 (2015).
48. Bliokh, K. Y., Smirnova, D. & Nori, F. Quantum spin Hall effect of light. *Science* **348**, 1448–1451 (2015).
49. Chern, R.-L. & Yu, Y.-Z. Chiral surface waves on hyperbolic-gyromagnetic metamaterials. *Opt. Express* **25**, 11801–11812 (2017).
50. Wang, L.-G., Wang, Z.-G., Zhang, J.-X. & Zhu, S.-Y. Realization of Dirac point with double cones in optics. *Opt. Lett.* **34**, 1510–1512 (2009).
51. Sakoda, K. Double Dirac cones in triangular-lattice metamaterials. *Opt. Express* **20**, 9925–9939 (2012).
52. Pendry, J. B., Holden, A. J., Stewart, W. J. & Youngs, I. Extremely low frequency plasmons in metallic mesostructures. *Phys. Rev. Lett.* **76**, 4773–4776 (1996).
53. Pendry, J. B., Holden, A. J., Robbins, D. J. & Stewart, W. J. Magnetism from conductors and enhanced nonlinear phenomena. *IEEE Trans. Microw. Theory Tech.* **47**, 2075–2084 (1999).
54. Bliokh, K. Y. & Nori, F. Transverse spin of a surface polariton. *Phys. Rev. A* **85**, 061801 (2012).
55. Gao, W. *et al*. Topological photonic phase in chiral hyperbolic metamaterials. *Phys. Rev. Lett.* **114**, 037402 (2015).

Acknowledgements
The authors thank Profs. C. T. Chan and Jensen Li at Hong Kong University of Science and Technology for valuable discussions. This work was supported in part by Ministry of Science and Technology under Contract No. MOST 105-2221-E-002-161-MY3.

Author Contributions
Y.Z.Y. derived the analytic formulae, conducted numerical simulations, and wrote the initial manuscript. R.L.C. proposed the research direction, supervised the work, and revised the manuscript. Both authors participated in the discussion.

Additional Information
Competing Interests: The authors declare no competing interests.

Publisher's note: Springer Nature remains neutral with regard to jurisdictional claims in published maps and institutional affiliations.